Yuan et al. *Microsystems & Nanoengineering* (2025)11:101
https://doi.org/10.1038/s41378-025-00923-5

Microsystems & Nanoengineering
www.nature.com/micronano

ARTICLE Open Access

Centrifugation-assisted lateral flow assay platform: enhancing bioassay sensitivity with active flow control

Hang Yuan[1], Ruiqi Yong[1], Wenwen Yuan[1,2], Quan Zhang[1,2], Eng Gee Lim[1,2], Yongjie Wang[3], Fuzhou Niu[4]✉ and Pengfei Song[1,2]✉

Abstract

Lateral flow assays (LFAs) are widely used in point-of-care testing (POCT) due to their simplicity and rapid operation. However, their reliance on passive capillary flow limits sensitivity, making it challenging to detect low-abundance biomarkers accurately. Approaches such as computer signal processing, chemical modification, and physical regulation have been explored to improve LFA sensitivity, but they remain limited by passive capillary-driven flow and uncontrollable flow rate. An alternative approach is to actively regulate fluid dynamics to optimize analyte binding and signal generation. The key challenge is to enhance LFA sensitivity while preserving compatibility with existing lateral flow strips (LFSs). Here, this study introduces a centrifugation-assisted LFA (CLFA) platform with smartphone-based result processing. This platform applies centrifugal force opposite to capillary flow, actively regulating fluid movement to optimize incubation time at the reaction zone and enhance detection performance. This approach increases signal intensity while maintaining a rapid detection process (5 min) and ensuring integration with traditional LFSs. As a proof-of-concept, the CLFA platform successfully detected human chorionic gonadotropin (hCG) and hemoglobin (Hb) in artificial urine without requiring custom-designed centrifugal discs or modified chromatography membranes. Its adaptability to diverse biomarkers and smartphone-based quantification make it a promising POCT tool, particularly in resource-limited settings.

Introduction

The applicability of point-of-care testing (POCT) devices in modern healthcare is expanding continuously, especially for home-based and resource-limited settings[1,2]. These devices provide simple, rapid, and highly targeted screening, reducing risks associated with centralized testing while enabling timely, personalized diagnostic information[3,4]. Because of the successful commercialization of paper-based lateral flow assays (LFAs) for home pregnancy tests, they have become one of the most widely used POCT formats due to their cost-effectiveness and user-friendliness[5,6]. LFAs primarily involve specific antibody-antigen immune reactions on lateral flow strips (LFSs), driven by capillary action, enabling rapid detection of biomarkers in bodily fluids such as urine and blood (~15 min)[6,7]. However, traditional LFAs normally rely on visual signal readouts resulting from the accumulation of gold nanoparticles (AuNPs), which limits their sensitivity and quantitative capability[8]. To address this, smartphone-based detection improves LFAs by providing automated, standardized result interpretation, reducing variability from visual assessment[9]. This cost-effective approach supports real-time data storage, remote consultation, and integration into digital health systems, making it especially suitable for resource-limited POCT[10].

Correspondence: Fuzhou Niu (fzniu@usts.edu.cn) or Pengfei Song (pengfei.song@xjtlu.edu.cn)
[1]School of Advanced Technology, Xi'an Jiaotong—Liverpool University, Suzhou 215123, China
[2]Department of Electrical Engineering and Electronics, University of Liverpool, Liverpool L69 7ZX, UK
Full list of author information is available at the end of the article
These authors contributed equally: Hang Yuan, Ruiqi Yong, and Wenwen Yuan.

Current efforts to improve LFA performance mainly focus on three approaches: computer signal processing, chemical modification, and physical regulation. The first approach involves hardware and algorithm development, such as image processing algorithms[9,10], and thermal imaging sensors[11,12]. However, complex signal processing may require significant computational resources and user training. This limits its applicability in resource-limited areas and among non-professional users. Additionally, the second one includes the use of chemical amplification strategies (*e.g.*, gold and silver enhancement methods[13,14], enzyme-based colorimetric amplification[15], and Cu^{+}-catalyzed click chemistry[16]) or newly synthesized tracers (*e.g.*, magnetic nanoparticles[17], graphene oxide[18], carbon nanotubes[19,20], cellulose nanobeads[21], fluorescent dyes[22], quantum dots[23]) to amplify detection signals. While these methods provide high sensitivity for LFA, the introduction of materials with specific optical, thermal, magnetic, and electrochemical properties may affect the stability and repeatability of specific detection and prolong the detection time, thereby increasing the burden on the user. The third strategy involves altering the pore size of paper-based substrates used in the LFSs, such as creating hybrid material by incorporating agarose into the LFS to regulate pore size for sample flow control[24]. Additionally, it includes constructing microstructures on the LFSs, such as wax-printed hydrophobic barriers or geometrically optimized microchannels[25,26], to alter sample flow and enhance LFA sensitivity. Although these methods help optimize the analyte-probe binding time by delaying fluid flow, the entire process is still passively driven by capillary forces and cannot actively adjust the flow rate. This may not adequately accommodate variations in liquid flow rates caused by different samples' viscosity and surface tension, affecting the improvement of LFA sensitivity and its applicability.

Therefore, active flow control has emerged as a promising strategy to enhance LFA sensitivity by overcoming the limitations of passive capillary-driven systems. Active regulation of fluid flow helps reduce inconsistencies from uneven dynamics, thereby improving stability, repeatability, and signal reliability. It also allows adjustments based on sample properties such as viscosity and surface tension, ensuring compatibility across various diagnostic scenarios, including urine and blood[27]. Previous studies have demonstrated the potential of centrifugal force in active flow regulation. For instance, Kainz et al. and Hwang et al. theoretically showed that centrifugal force effectively controls flow through chromatography membranes[27,28]. Additionally, Shen et al. further advanced this concept by integrating specially shaped chromatography membranes into centrifugal microfluidic discs, significantly enhancing sensitivity in detecting prostate-specific antigens[29,30]. These studies highlight the ability of centrifugal techniques to reduce flow rates, extend incubation times, and improve analyte binding efficiency. These are key factors for enhancing detection sensitivity. However, existing methods often rely on custom-designed centrifugal discs or modified chromatography membranes, which introduce design complexities, increase manufacturing costs, and limit compatibility with standard LFSs. A universal centrifugation-assisted platform is therefore needed to enhance biosensing sensitivity without modifying traditional LFSs. Such a platform supports non-professional users, enabling convenient, accurate testing and broad diagnostic applicability.

This study presents a centrifugation-assisted lateral flow assay (CLFA) platform that enhances bioassay sensitivity. This platform can be directly used with traditional LFSs without the need for additional design or preparation. The CLFA platform optimizes the incubation time of the sandwich immune complex on reaction lines by rotating the centrifugal disc at optimized rotation speeds and time. This generates adjustable centrifugal forces to regulate the capillary-driven liquid flow rate. As a proof-of-concept, we detected different concentrations of human chorionic gonadotropin (hCG) and hemoglobin (Hb) in artificial urine on the CLFA platform. hCG, widely used in pregnancy diagnostics, serves as a benchmark for LFA performance[31]. In addition, Hb, a key biomarker for fecal occult blood screening, demonstrates the platform's ability to detect low-abundance analytes[32]. Additionally, we developed a smartphone application to capture the LFS results on the platform using the phone's built-in camera. The results showed that the CLFA platform achieved lower limits of detection (LoDs) for hCG and Hb than the commercial LFSs (25 mIU mL^{-1} and 200 ng mL^{-1}, respectively)[31,32]. Moreover, the prepared LFSs exhibited high specificity, effectively minimizing interference from non-target protein biomarkers. Our smartphone-based CLFA platform enhances LFA sensitivity through active flow regulation, providing an automated and user-friendly detection method with strong potential for advancing POCT development.

Results and discussions

Design and working principles of the CLFA platform

The conceptual comparison shown in Fig. 1a highlights the advantages of active flow control in the CLFA platform over traditional LFAs. For the design of our CLFA platform, as shown in Fig. 1b, a dismantled gearbox DC motor is mounted onto the 3D-printed base through its threaded hole. Two layers of centrifuge discs made of PMMA are fixed onto the main shaft of the motor through the motor flange. The cartridge with internal dimensions matching the LFS size is securely placed in a slot of the centrifuge disc that matches its outer dimensions. The orientation of the slot is aligned radially with

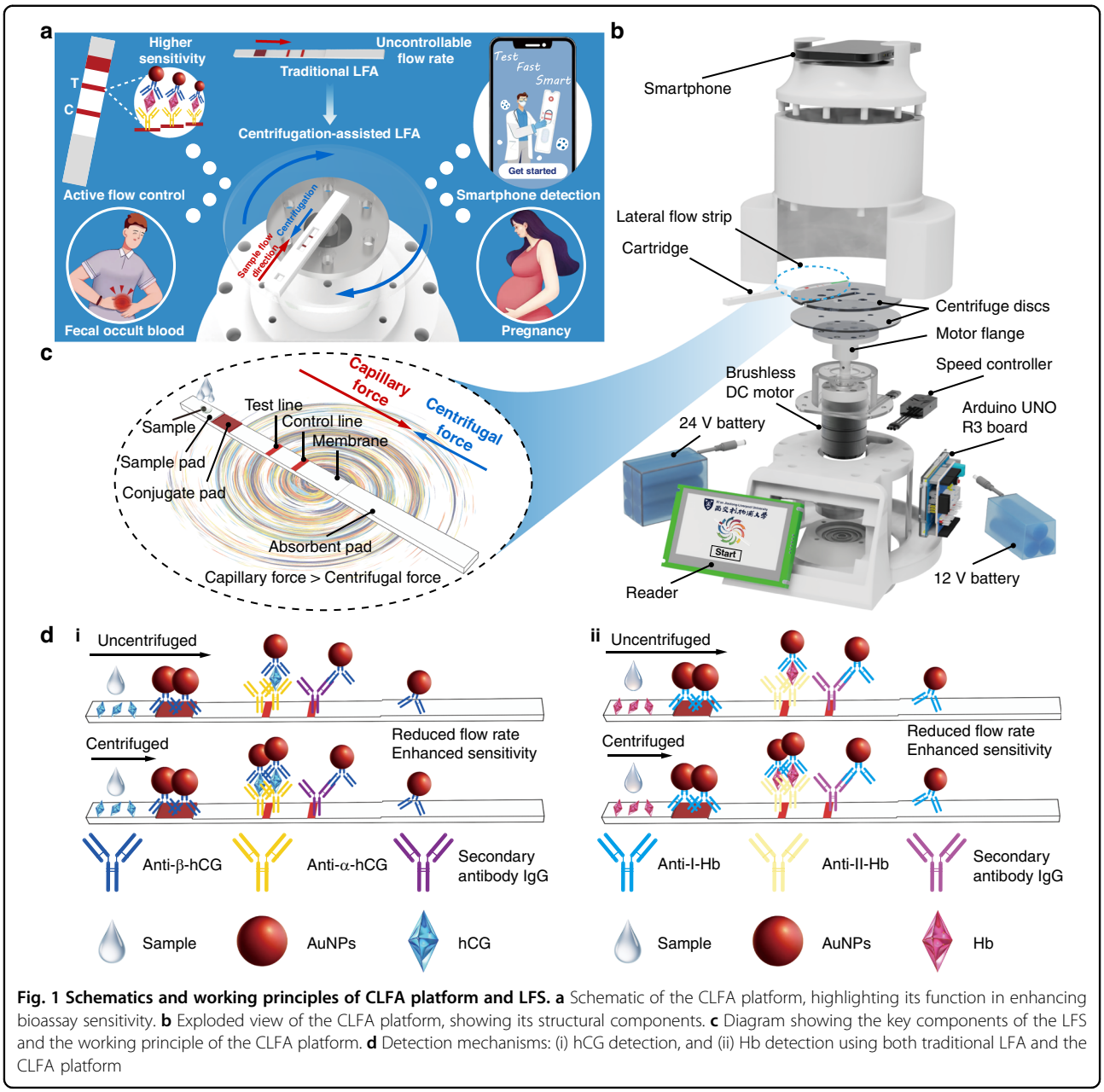

Fig. 1 Schematics and working principles of CLFA platform and LFS. a Schematic of the CLFA platform, highlighting its function in enhancing bioassay sensitivity. **b** Exploded view of the CLFA platform, showing its structural components. **c** Diagram showing the key components of the LFS and the working principle of the CLFA platform. **d** Detection mechanisms: (i) hCG detection, and (ii) Hb detection using both traditional LFA and the CLFA platform

the centrifuge discs. Except for 70% of the length of the absorbent pad (14 mm), all components of the LFS are aligned along a single radial axis to ensure uniform centrifugal force during detection. The specific dimensions of the centrifuge discs and the cartridge are shown in Fig. S1. Additionally, the platform includes a DC motor speed controller and both 24 V and 12 V batteries. The CLFA device is controlled by Arduino and interacts with the reader. All components are enclosed in 3D-printed housings. The smartphone is placed on the 3D-printed phone holder above the device, with its camera aligned to a hole in the center of the housing. This allows for image capture of LFS results from a distance of ~35 mm.

The movement of the liquid sample on the LFS is passively driven by the capillary force generated by the absorbent pad, depending on the specific structure and material of the LFS[33,34]. Adjusting the motor rotation speed enables the centrifuge discs to spin at an optimized rate, generating a controlled centrifugal force. The outward centrifugal force counteracts the inward-directed capillary flow[28]. As a result, fluid movement on the LFS is governed by the interplay between capillary action and centrifugal force. At lower rotation speeds (<800 rpm), capillary action dominates fluid movement after the liquid is dispensed onto the sample pad. This drives the fluid through the conjugate pad and nitrocellulose (NC)

membrane to the absorbent pad, as shown in Fig. 1c and S2a. This reduced flow rate extends the reaction time, facilitating the formation of stable sandwich immune complexes at the reaction lines.

The mechanisms for detecting hCG and Hb on the CLFA platform are illustrated in Fig. 1d–i and d–ii, respectively. In traditional LFAs, the analyte-antibody complex migrates along the LFS via capillary action and is captured at the T line by immobilized antibodies, forming a visible signal. On the CLFA platform, a greater number of immune complexes formed at the T line under the influence of centrifugal force. For the performance evaluation of the CLFA platform, firstly, different concentrations of hCG and Hb standard solutions were prepared by diluting hCG antigen and Hb antigen in artificial urine, respectively. Secondly, a fixed volume (60 μL) of standard solution was dropped onto the LFS, and the CLFA platform was started at a fixed rotation speed depending on the sample (hCG or Hb standard solutions). Finally, after the platform stopped rotating at the same fixed time (180 s), the signal intensities of the T line and C line were read using a smartphone, and the relative intensities were calculated through a smartphone application. Both the rotation speed and rotation time were optimized. The entire CLFA process was completed with a stable result displayed within 5 min (180 s centrifugation followed by 120 s rest), as shown in Video S1, with all experiments conducted at room temperature. This duration offers higher detection efficiency compared to traditional LFAs (typically 15 min). It also minimizes variability due to sample evaporation by standardizing the capture time and may improve throughput for large-scale screenings[9].

Centrifugation parameter optimization

We optimized the performance of the CLFA platform by fine-tuning centrifugation parameters to regulate the liquid flow rate on the LFS, thereby enhancing the detection sensitivity for hCG and Hb. Due to differences in viscosity and surface tension between the two analytes, separate optimization processes were conducted. The centrifugation process was divided into two stages to optimize analyte binding and increase the relative intensity of the LFS. The first stage (1st stage) occurs before the liquid sample reaches the T line, where a reduced flow rate extends incubation time and facilitates analyte–antibody binding, thereby enhancing immune complex formation and detection sensitivity. The second stage (2nd stage) takes place after the sample passes the T line, where centrifugal force aids in removing excess reagents and unbound substances, reducing non-specific signals.

We investigated the effects of different rotation speeds and time ratios. The effective rotation speed range for the CLFA platform was determined to be 100-800 rpm, with tests performed at 100 rpm intervals. A minimum speed of 100 rpm was required to overcome the initial inertia of the centrifuge discs. In contrast, speeds above 800 rpm caused reverse flow toward the sample pad, disrupting normal progression through the LFS (Fig. S2b). To optimize timing, we evaluated three time ratios of the two-stage centrifugation (1:3, 1:1, and 3:1), while maintaining a fixed total centrifugation time of 180 s. Additionally, intermediate rotation speeds of 400 rpm and 500 rpm were selected for the 1st stage to systematically explore flow regulation across both lower and higher speeds during the 2nd stage.

We conducted performance evaluations using samples of equal concentrations (hCG: 400 mIU mL^{-1}, Hb: 200 ng mL^{-1}) and a fixed volume (60 μL) at various rotation speeds and time ratios, measuring relative intensities in five replicates. The results showed that for hCG detection, the optimal parameters were 500 rpm for 135 s in the 1st stage (time ratio 3:1), followed by 600 rpm for 45 s in the 2nd stage (Fig. 2a, b). For Hb detection, the optimal parameters were 400 rpm for 90 s in the 1st stage (time ratio 1:1), followed by 300 rpm for 90 s in the 2nd stage (Fig. 2c, d). Under these optimized conditions, the CLFA platform exhibited higher relative intensity compared to traditional LFAs, attributed to reduced sample retention in the sample and conjugate pads and improved reagent utilization efficiency[35]. By controlling flow rates, the platform extends molecular interaction time for immune complex formation. In contrast, traditional LFSs tend to lose gold-labeled probes in the early stages because LFSs are soaked in the sample or washed away[29], resulting in lower reaction efficiency and diminished signal intensity. These optimized centrifugation parameters were subsequently applied for the detection of hCG and Hb.

Development of the LFS reading smartphone application

Figure 3a shows photos of the centrifuge discs within the CLFA platform and the positioning of the smartphone. The setup creates a closed, light-shielding environment, ensuring imaging consistency and preventing interference from external light sources to enhance the reliability of image acquisition. The phone was set to automatically adjust shooting parameters, including white balance, aperture value, shutter speed, and sensitivity. We developed an LFS reading smartphone application that provides users with quantitative results of hCG and Hb concentrations. Firstly, users launch the start interface (Fig. 3b-i) to enter the registration interface (Fig. 3b-ii). Successful registration requires the use of a preset verification code to ensure information security. Secondly, after registration, users log in (Fig. 3b-iii); if they already have a registered account, they can directly log in. Thirdly, users upload an LFS photo, captured by the phone's

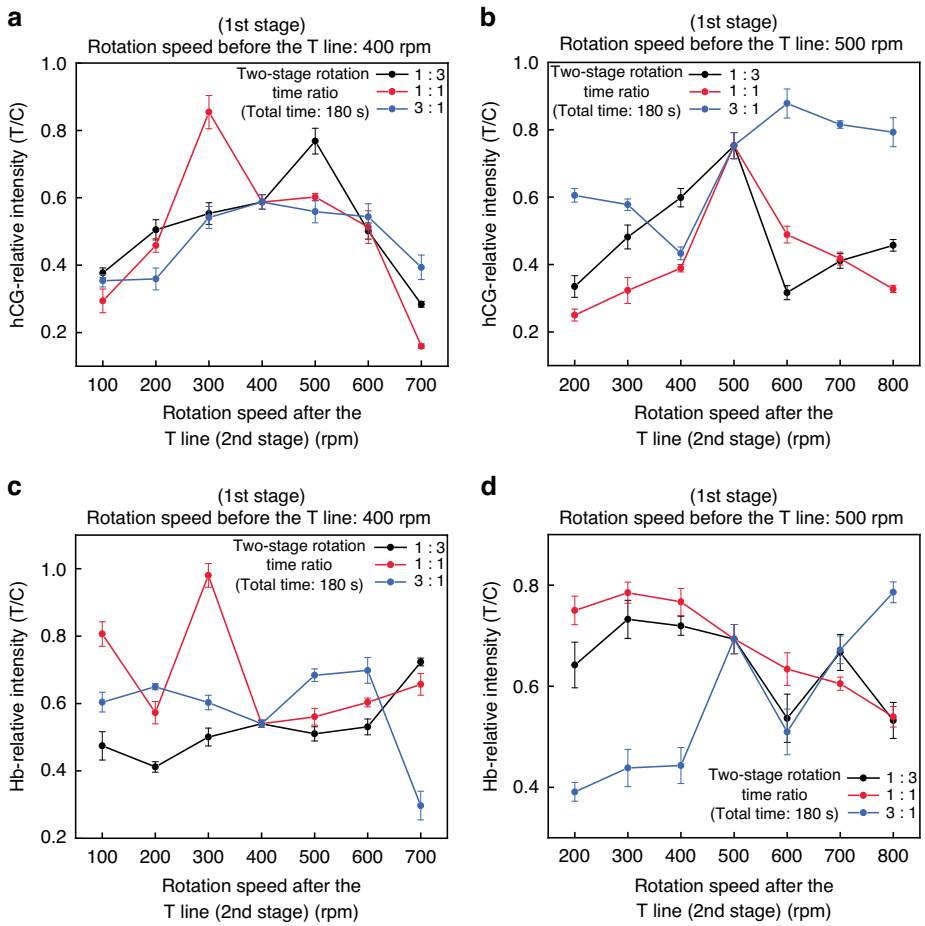

Fig. 2 Optimization of centrifugation parameters for hCG and Hb detection ($n = 5$). a, **b** Effects of two-stage rotation speeds and time ratios on the relative intensity of hCG detection (400 mIU mL^{-1}). First-stage rotation speeds were set at 400 rpm (**a**) and 500 rpm (**b**), while second-stage speeds were varied. **c**, **d** Effects of two-stage rotation speeds and time ratios on the relative intensity of Hb detection (200 ng mL^{-1}). First-stage rotation speeds were set at 400 rpm (**c**) and 500 rpm (**d**), with varying second-stage speeds. The relative intensity (T/C) is defined as the ratio of the peak values of the T line and C line. In all cases, the total centrifugation time was fixed at 180 s, with three different time ratios (1:3, 1:1, 3:1) explored for the two stages

camera, from the gallery for processing, including cropping and rotating. Then, using the manual framing function on the photo, the areas of T line and C line were selected respectively to allow signal profiles to be represented along the LFS (Fig. 3b-iv). Fourthly, users obtain the signals from the T line, C line, and background (S_T, S_C, and $S_{background}$). The relative intensities of LFSs for hCG and Hb detection are calculated automatically, respectively (Fig. 3b-v and b-vii). In this process, the background signal ($S_{background}$) is read from an area between the T line and the C line on the LFS, which is free of specific binding interactions. The raw signals of both the T line and C line (S_T and S_C) were subtracted from this background signal to obtain the corrected signal intensity, also referred to as the peak value ($S_{T,\,peak}$ and $S_{C,\,peak}$). In the grayscale representation of LFS, the background signal typically exhibits higher intensity values. The relative intensity ($I_{relative}$) is the ratio of the peak values of the T line and C line, aiming to eliminate interference from background noise (Eq. 1)[35]. Finally, users select the target biomarker, and the smartphone interface then automatically calculates and displays the corresponding concentration of hCG or Hb using pre-established sigmoidal curves (Fig. 3b–vi and b–viii).

$$S_{T,\,peak} = S_{background} - S_T \tag{1a}$$

$$S_{C,\,peak} = S_{background} - S_C \tag{1b}$$

$$I_{relative} = S_{T,\,peak}/S_{C,\,peak} \tag{1c}$$

Where $S_{T,\,peak}$, and $S_{C,\,peak}$ represent the peak values of the T-line and C-line, respectively, S_T and S_C are their raw

Fig. 3 Smartphone-assisted CLFA platform and workflow of the LFS reading application. a Photos of the CLFA platform, showing the interior centrifuge discs used for active flow control. **b** Workflow of the smartphone application for LFS reading: (i) Start interface for initiating the application. (ii) User registration page for creating an account. (iii) User login page for accessing the application. (iv) Signal reading interface for the T and C lines of the LFS, including tools for image cropping and rotation. (v, vii) Interface for calculating the relative intensities of LFSs for hCG and Hb detection, respectively. (vi, viii) Interface displaying the final concentration results of hCG and Hb, after selecting the target biomarker. The smartphone application automatically performs quantification using pre-fitted sigmoidal calibration curves

signal intensities, and $S_{background}$ denotes the background signal intensity.

Characterization of AuNPs and gold-labeled probes

The quality of AuNPs and the gold-labeled probe is critical for the performance of LFSs. Therefore, to confirm the adsorption of Anti-β-hCG and Anti-I-Hb onto the surface of AuNPs, several characterizations were demonstrated. The protein adsorb onto the AuNPs surface through strong ionic interactions beyond the thiol-Au link[36]. Consequently, its characteristic peak can be detected by UV-vis. Figure 4a depicts the UV-vis absorption spectra of bare AuNPs, the incubated Anti-β-hCG@AuNPs, and Anti-I-Hb@AuNPs. The results showed the bare AuNPs exhibited a prominent surface plasmon resonance (SPR) absorption peak at 530 nm. Notably, Anti-β-hCG@AuNPs and Anti-I-Hb@AuNPs both exhibited distinct SPR peaks (536 nm and 541 nm) with a red shift of 6 nm and 11 nm, respectively. This red shift was attributed partly to the increased nanoparticle diameter and mostly to the change in the boundary of AuNPs, which strongly influenced its SPR peak[9,37,38], indicating the successful conjugation of antibodies and AuNPs. Moreover, according to the ref. [39], the relationship between the diameter of bare AuNPs and their SPR peak wavelength is shown in Table S1. The optimal size of AuNPs is crucial for signal strength and stability during centrifugation[39]. AuNPs with larger diameters generate stronger signals, but they tend to sediment more readily[29,40,41]. Hence, to achieve a balance between signal intensity and sedimentation, we selected AuNPs with a diameter of ~40 nm[29]. Figure S3 displays the UV-vis absorption spectra of bare AuNPs with different diameters prepared in our study.

Transmission electron microscopy (TEM) images of bare AuNPs, Anti-β-hCG@AuNPs, and Anti-I-Hb@AuNPs reveal their spherical morphology with good dispersibility and homogeneity, as shown in Fig. 4b-i, c-i and d-i, respectively. Figure 4b-ii shows that bare AuNPs have a relatively uniform size, with an average diameter of 39.83 ± 2.56 nm. A thin layer of water-like striation indistinctly surrounds the surface of the gold-labeled

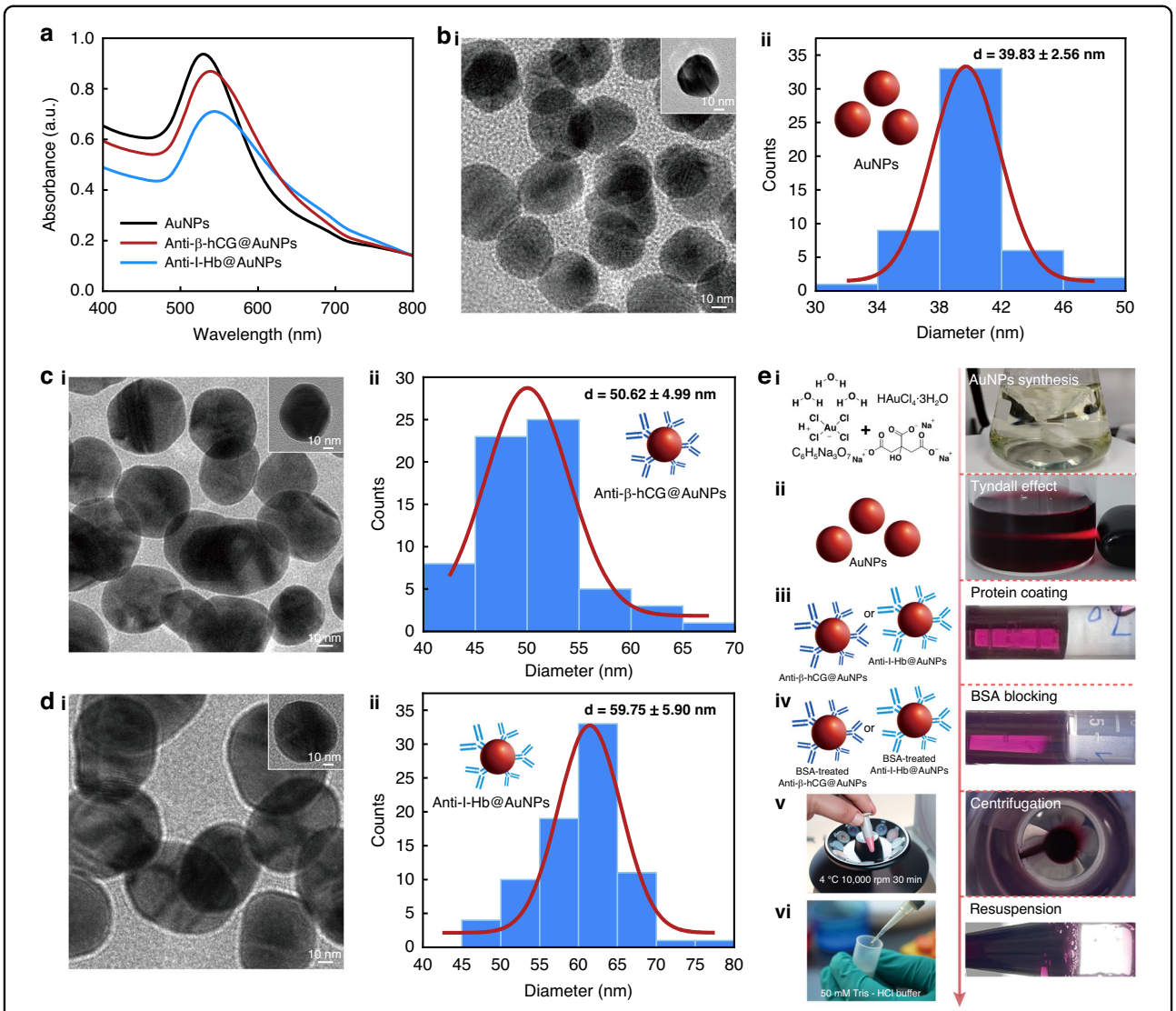

Fig. 4 Characterization and preparation process of AuNPs and gold-labeled probes. a UV-vis absorption spectra of AuNPs, Anti-β-hCG@AuNPs, and Anti-I-Hb@AuNPs, showing shifts due to antibody conjugation. **b** (i) TEM image and (ii) size distributions of AuNPs ($d = 39.83 \pm 2.56$ nm). **c** (i) TEM image and (ii) size distributions of Anti-β-hCG@AuNPs ($d = 50.62 \pm 4.99$ nm). **d** (i) TEM image and (ii) size distributions of Anti-I-Hb@AuNPs ($d = 59.75 \pm 5.90$ nm). **e** Schematic and photos of the preparation process: (i) AuNPs synthesized using sodium citrate reduction. (ii) Tyndall effect observed in AuNPs. (iii) Antibody protein-coated AuNPs. (iv) BSA blocks nonspecific binding sites. (v) Centrifugation at 10,000 rpm and 4 °C for 30 min to remove free antibodies. (vi) Resuspension of gold-labeled probes in 50 mM Tris-HCl buffer

probes, indicating successful antibody modification on the AuNPs surface. After protein coating, the complexes of Anti-β-hCG@AuNPs and Anti-I-Hb@AuNPs exhibited an average diameter of 50.62 ± 4.99 nm and 59.75 ± 5.90 nm, respectively. Size distributions of these gold-labeled probes are illustrated in Fig. 4c-ii and d-ii, affirming the stability of the synthesized nanoconjugates. The variation in hydrodynamic diameter is attributed to their adsorbed layers. The mutual confirmation between TEM images and UV-vis spectra ultimately confirms the successful generation of specific-sized core-satellite sandwich structures during the preparation process. The preparation and functionalization steps of the gold-labeled probes are illustrated in Fig. 4e(i-vi) and described in detail in the supplemental information.

The adsorption of protein onto AuNPs primarily depended on the pH of the solution, as protein bond more firmly with AuNPs near their isoelectric point or under alkaline conditions[42]. Figure 5a-i and b-i demonstrate that during the preparation of Anti-β-hCG@AuNPs and Anti-I-Hb@AuNPs, significant aggregation occurs when the pH is below 6.5 and 7.0, respectively. This aggregation results in a color change to colorless (due to their precipitation) and purple (due to a shift and broadening of

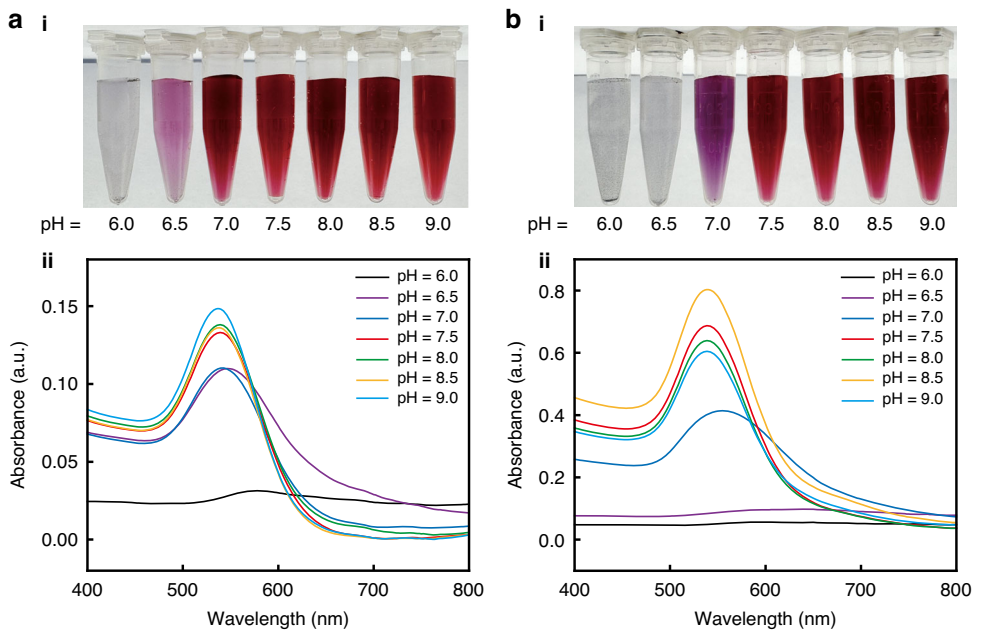

Fig. 5 Effects of pH on the stability and optical properties of gold-labeled probes. a Anti-β-hCG@AuNPs: (i) Photos showing the color changes under different pH conditions (6.0–9.0). (ii) Corresponding UV-vis absorption spectra. **b** Anti-I-Hb@AuNPs: (i) Photos showing the color changes under different pH conditions (6.0–9.0). (ii) Corresponding UV-vis absorption spectra

the plasmonic peak), indicating instability. These results suggest that antibodies cannot be reliably conjugated to AuNPs at pH levels below the isoelectric point of protein.

In contrast, within the pH ranges of 7.0–9.0 for Anti-β-hCG@AuNPs and 7.5–9.0 for Anti-I-Hb@AuNPs, the colors remain dark red, indicating stable conjugation of the gold-labeled probes. Furthermore, as shown in Fig. 5a-ii and b-ii, the SPR peak positions of the stable conjugates exhibit slight redshifts at these pH levels, attributed to an increase in the hydrodynamic diameter caused by successful antibody conjugation[35]. Based on these results, we identified pH = 7.5 as the optimal condition for preparing the gold-labeled probes (Anti-β-hCG@AuNPs and Anti-I-Hb@AuNPs). This pH optimization improves the gold-labeled probes stability, thereby enhancing LFS performance and the reliability of colorimetric signal generation.

Specificity test

In the experiments for hCG detection, bovine serum albumin (BSA) and a common interference, luteinizing hormone (LH), were selected to evaluate the specificity of the LFSs (Fig. 6a-i)[9,43]. For Hb detection, BSA, along with common interferences, bovine hemoglobin (BHb), and horseradish peroxidase (HRP), were chosen (Fig. 6b-i)[44]. The interference concentrations (1 μg mL^{-1}) were higher than those of the target biomarkers (hCG and Hb). The results showed negligible signals for these protein interferences on the LFSs for hCG and Hb detection (Fig. 6a-ii and b-ii), indicating that they did not affect the assay specificity.

Furthermore, the optimized rotation speeds and time ratios identified in Fig. 2 were applied for centrifugation. After centrifugation, despite the presence of interfering substances, the specificity of the hCG and Hb LFSs was maintained, with no false-positive signals observed on the T line (Fig. 6c-i and d-i). The peak values of the T line for hCG and Hb detection were enhanced, respectively, demonstrating improved signal intensity on our CLFA platform (Fig. 6c-ii and d-ii). Even at low concentrations of hCG (400 mIU mL^{-1}) and Hb (50 ng mL^{-1}), the centrifuged LFSs exhibited sensitive responses, showing clear T line signals similar to those observed without interference. These results, together with the data in Table S2, confirm that the prepared LFSs exhibit robust specificity and reliably detect hCG and Hb under varying conditions.

Performance evaluation of CLFA platform for hCG and Hb detection

To evaluate the performance of the CLFA platform, LFSs prepared using our standardized method served as the control group. Following a 1-month stability assessment, our LFSs demonstrated reliable and relatively consistent results, making them suitable for this comparative study (Table S3 and Fig. S5). Meanwhile, LFSs centrifuged on the CLFA platform served as the experiment group. Performance evaluation included the

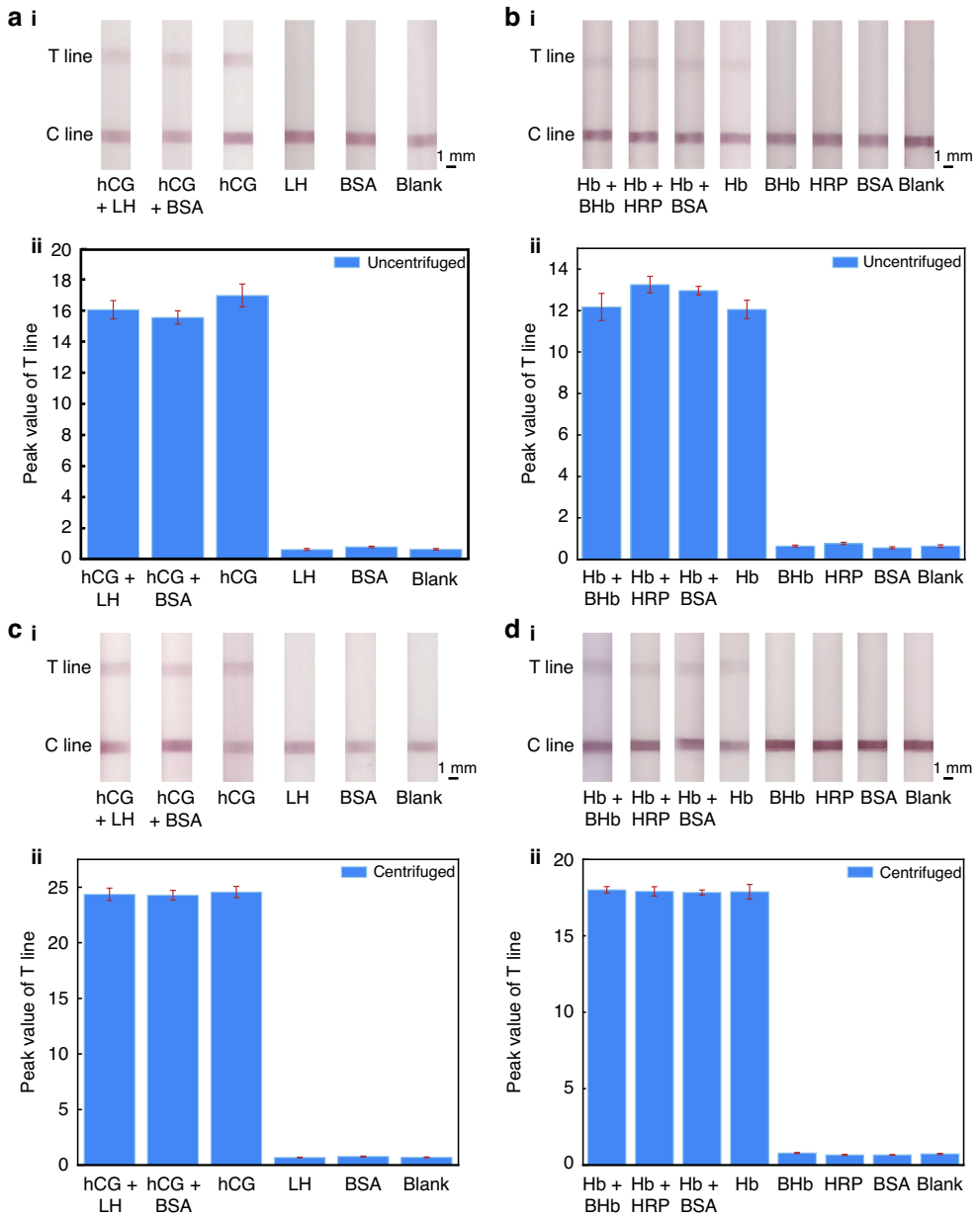

Fig. 6 Specificity evaluation of LFSs for hCG and Hb detection ($n = 5$). a Uncentrifuged hCG detection: (i) Photos of LFSs under different conditions. The hCG concentration is 400 mIU mL^{-1}, and potential interfering substances included LH and BSA at 1 μg mL^{-1}. (ii) Peak values of the T line. **b** Uncentrifuged Hb detection: (i) Photos of LFSs under different conditions. The Hb concentration is 50 ng mL^{-1}, and potential interfering substances included BHb, HRP, and BSA at 1 μg mL^{-1}. (ii) Peak values of the T line. **c** Centrifuged hCG detection: (i) Photos of LFSs under different conditions after centrifugation. (ii) Peak values of the T line. **d** Centrifuged Hb detection: (i) Photos of LFSs under different conditions after centrifugation. (ii) Peak values of the T line

detection of hCG and Hb using the LFSs, with results collected via the same smartphone. Different concentrations of hCG (0–10,000 mIU mL^{-1}) and Hb (0–1500 ng mL^{-1}) standard solutions were obtained through artificial urine dilution, with each concentration tested five times using the LFSs to calculate the mean relative intensity (Fig. 7a-i and b-i). Within the target concentration range, we utilized a four-parameter logistic curve (sigmoidal curve) to obtain data fitting in Origin software. According to the references[35,45], we conservatively calculated the LoD of the LFA using a widely accepted method, which involves adding three times the standard deviation (S_d) to the blank value (S_b). The curve-fitting standard equation, coefficient of determination

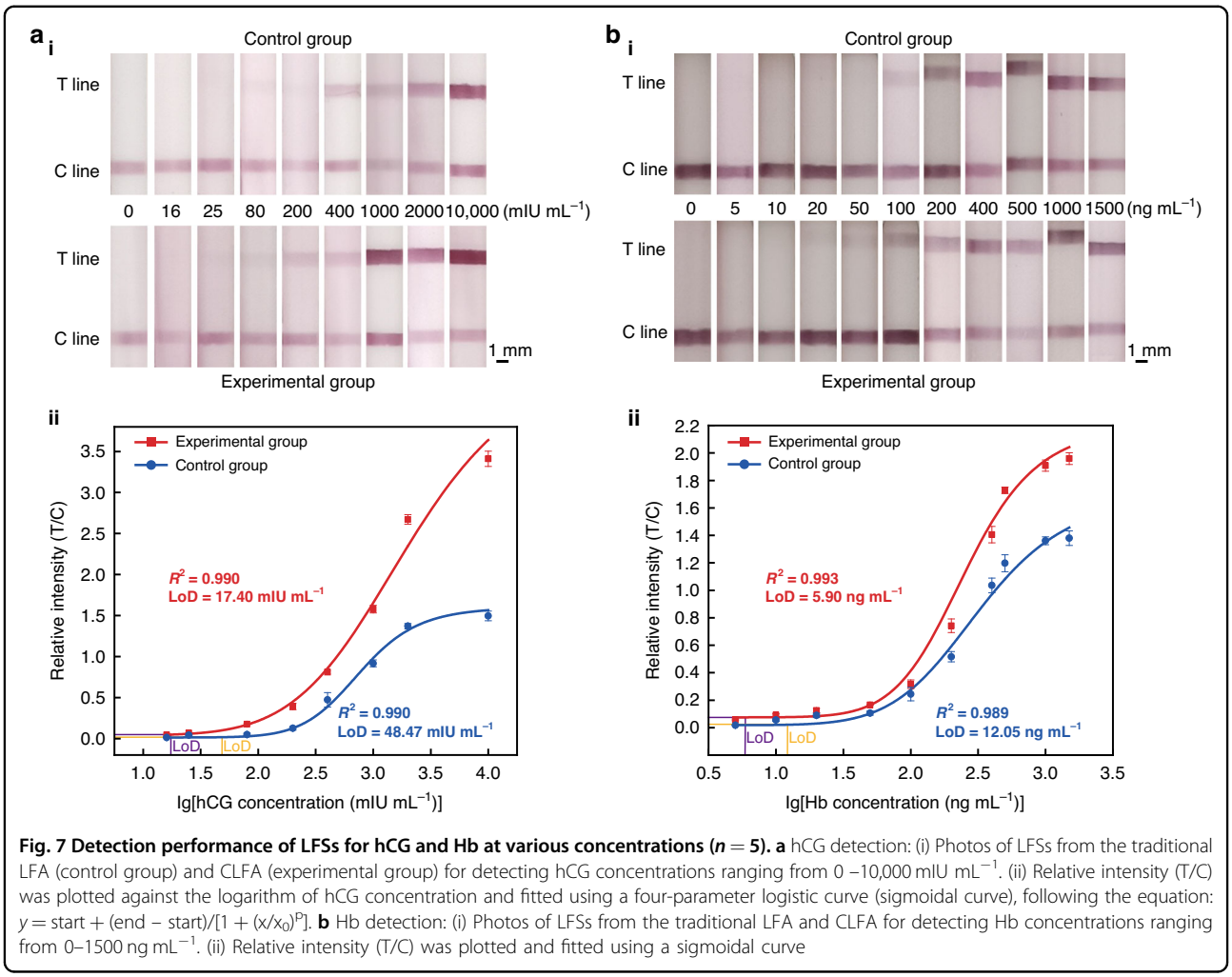

Fig. 7 Detection performance of LFSs for hCG and Hb at various concentrations ($n = 5$). a hCG detection: (i) Photos of LFSs from the traditional LFA (control group) and CLFA (experimental group) for detecting hCG concentrations ranging from 0 –10,000 mIU mL^{-1}. (ii) Relative intensity (T/C) was plotted against the logarithm of hCG concentration and fitted using a four-parameter logistic curve (sigmoidal curve), following the equation: $y = \text{start} + (\text{end} - \text{start})/[1 + (x/x_0)^P]$. **b** Hb detection: (i) Photos of LFSs from the traditional LFA and CLFA for detecting Hb concentrations ranging from 0–1500 ng mL^{-1}. (ii) Relative intensity (T/C) was plotted and fitted using a sigmoidal curve

Table 1 Detection results of hCG and Hb samples using traditional LFA and CLFA ($n = 5$)

Sample	Method	Standard curve	R^2	LoD
hCG	Traditional LFA	$y = 1.59 - 1.57/[1 + (x/2.85)^{10.92}]$	0.990	48.47 mIU mL^{-1}
	CLFA	$y = 4.72 - 4.68/[1 + (x/3.32)^{6.42}]$	0.990	17.40 mIU mL^{-1}
Hb	Traditional LFA	$y = 1.71 - 1.69/[1 + (x/2.51)^{7.49}]$	0.989	12.05 ng mL^{-1}
	CLFA	$y = 2.21 - 2.13/[1 + (x/2.41)^{8.98}]$	0.993	5.90 ng mL^{-1}

(R^2), and LoD are shown in Table 1. The LoD values for hCG and Hb detection using the CLFA platform are 17.40 mIU mL^{-1} and 5.90 ng mL^{-1}, respectively, which are both higher than the LoD of the control group (48.47 mIU mL^{-1} and 12.05 ng mL^{-1}). All four groups exhibited high R^2 values (above 0.98), indicating a strong correlation between analyte concentration and relative intensity. Therefore, as shown in Fig. 7a-ii and b-ii, our CLFA platform exhibits higher sensitivity than traditional LFA for hCG and Hb detection. In the future, this platform can be adjusted and expanded to detect more biomarkers, with the potential to further advance POCT applications.

Conclusion

In this study, we developed a smartphone-assisted CLFA platform to enhance the sensitivity of bioassays. This platform simply requires placing the traditional LFS into the centrifuge disc for automatic detection. By adjusting the centrifugal force, the platform can reduce

the liquid flow rate at the reaction line, thereby optimizing the incubation time of the immune complex. Unlike the passively driven LFAs that rely solely on capillary action, this process enables active control of the biomarker assay process. Furthermore, we developed a smartphone application that allows non-professional users to obtain results from LFSs within 5 minutes using a user-friendly interface. Under optimized centrifugal conditions, we detected one of the biomarkers for pregnancy (hCG) and fecal occult blood (Hb) in artificial urine. Compared to traditional LFAs, the LoDs for hCG and Hb on our platform were reduced by 64% and 51%, respectively. This improved sensitivity is also attributed to more efficient utilization of the sample, reducing retention in the sample pad or conjugate pad. In the future, by adjusting centrifugal parameters, the application of this platform could be extended to the detection of more biomarkers, potentially promoting the development of high-sensitivity POCT devices.

Acknowledgements
The authors acknowledge the financial support from the programs of the Natural Science Foundation of the Jiangsu Higher Education (24KJB460030), and XJTLU RDF project (RDF-21-02-076). This work is also partially supported by the XJTLU AI University Research Centre, Jiangsu Province Engineering Research Centre of Data Science and Cognitive Computation at XJTLU, and the SIP AI innovation platform (YZCXPT2022103). This work also acknowledges Jiangsu Provincial Outstanding Youth Program (BK20230072), Suzhou Industrial Foresight and Key Core Technology Project (SYC2022044), and grants from Jiangsu QingLan Project and Jiangsu 333 high-level talents.

Author details
[1]School of Advanced Technology, Xi'an Jiaotong—Liverpool University, Suzhou 215123, China. [2]Department of Electrical Engineering and Electronics, University of Liverpool, Liverpool L69 7ZX, UK. [3]School of Science, Harbin Institute of Technology, Shenzhen 518055, China. [4]School of Mechanical Engineering, Suzhou University of Science and Technology, Suzhou 215009, China

Author contributions
Hang Yuan: Writing—original draft, Writing—review and editing, Visualization, Methodology, Formal analysis, Data curation, Conceptualization. Ruiqi Yong: Writing—original draft, Writing—review and editing, Visualization, Methodology, Formal analysis, Data curation, Conceptualization. Wenwen Yuan: Writing—original draft, Writing—review and editing, Methodology, Conceptualization. Quan Zhang: Project administration, Methodology, Conceptualization. Eng Gee Lim: Project administration, Visualization, Conceptualization. Yongjie Wang: Methodology, Conceptualization. Fuzhou Niu: Writing—original draft, Writing—review and editing, Project administration, Funding acquisition, Supervision. Pengfei Song: Writing—original draft, Writing—review and editing, Project administration, Funding acquisition, Conceptualization, Supervision.

Data availability
The original contributions presented in the study are included in the article. Further inquiries can be directed to the corresponding authors.

Competing interests
The authors declare no competing interests.

Supplementary information The online version contains supplementary material available at https://doi.org/10.1038/s41378-025-00923-5.

Received: 7 September 2024 Revised: 7 February 2025 Accepted: 4 March 2025
Published online: 22 May 2025

References

1. Luppa, P. B., Müller, C., Schlichtiger, A. & Schlebusch, H. Point-of-care testing (POCT): current techniques and future perspectives. *TrAC Trends Anal. Chem.* **30**, 887–898 (2011).
2. Syedmoradi, L. et al. Point of care testing: the impact of nanotechnology. *Biosens. Bioelectron.* **87**, 373–387 (2017).
3. St John, A. & Price, C. P. Existing and emerging technologies for point-of-care testing. *Clin. Biochem. Rev.* **35**, 155 (2014).
4. McPartlin, D. A. & O'Kennedy, R. J. Point-of-care diagnostics, a major opportunity for change in traditional diagnostic approaches: potential and limitations. *Expert Rev. Mol. Diagnostics* **14**, 979–998 (2014).
5. Leuvering, J. H., Thal, P., van der Waart, M. & Schuurs, A. Sol particle immunoassay (SPIA). *J. Immunoass.* **1**, 77–91 (1980).
6. Posthuma-Trumpie, G. A., Korf, J. & van Amerongen, A. Lateral flow (immuno) assay: its strengths, weaknesses, opportunities and threats. A literature survey. *Anal. Bioanal. Chem.* **393**, 569–582 (2009).
7. Li, J. & Macdonald, J. Multiplexed lateral flow biosensors: technological advances for radically improving point-of-care diagnoses. *Biosens. Bioelectron.* **83**, 177–192 (2016).
8. Nguyen, V.-T., Song, S., Park, S. & Joo, C. Recent advances in high-sensitivity detection methods for paper-based lateral-flow assay. *Biosens. Bioelectron.* **152**, 112015 (2020).
9. Zhang, T. et al. A smartphone-based rapid quantitative detection platform for lateral flow strip of human chorionic gonadotropin with optimized image algorithm. *Microchem. J.* **157**, 105038 (2020).
10. Duan, S. et al. Automatic offline-capable smartphone paper-based microfluidic device for efficient biomarker detection of Alzheimer's disease,. *Anal. Chim. Acta* **1308**, 342575 (2024).
11. Ojaghi, A., Pallapa, M., Tabatabaei, N. & Rezai, P. High-sensitivity interpretation of lateral flow immunoassays using thermophotonic lock-in imaging. *Sens. Actuators A. Phys.* **273**, 189–196 (2018).
12. Qin, Z. et al. Significantly improved analytical sensitivity of lateral flow immunoassays by using thermal contrast. *Angew. Chem. Int. Ed.* **51**, 4358–4361 (2012).
13. Rodríguez, M. O., Covián, L. B., García, A. C. & Blanco-López, M. C. Silver and gold enhancement methods for lateral flow immunoassays. *Talanta* **148**, 272–278 (2016).
14. Kim, W., Lee, S. & Jeon, S. Enhanced sensitivity of lateral flow immunoassays by using water-soluble nanofibers and silver-enhancement reactions. *Sens. Actuators B. Chem.* **273**, 1323–1327 (2018).
15. Parolo, C., de la Escosura-Muñiz, A. & Merkoçi, A. Enhanced lateral flow immunoassay using gold nanoparticles loaded with enzymes. *Biosens. Bioelectron.* **40**, 412–416 (2013).
16. Wang, D., Ge, C., Wang, L., Xing, X. & Zeng, L. A simple lateral flow biosensor for the rapid detection of copper (II) ions based on click chemistry. *Rsc Adv.* **5**, 75722–75727 (2015).
17. Razo, S. C. et al. Double-enhanced lateral flow immunoassay for potato virus X based on a combination of magnetic and gold nanoparticles. *Anal. Chim. acta* **1007**, 50–60 (2018).
18. Shirshahi, V., Tabatabaei, S. N., Hatamie, S. & Saber, R. Functionalized reduced graphene oxide as a lateral flow immuneassay label for one-step detection of Escherichia coli O157: H7. *J. Pharm. Biomed. Anal.* **164**, 104–111 (2019).
19. Sun, W. et al. A novel multi-walled carbon nanotube-based antibody conjugate for quantitative and semi-quantitative lateral flow assays. *Biosci. Biotechnol., Biochem.* **81**, 1874–1882 (2017).
20. Yao, L. et al. MWCNTs based high sensitive lateral flow strip biosensor for rapid determination of aqueous mercury ions. *Biosens. Bioelectron.* **85**, 331–336 (2016).
21. Sakurai, A. et al. Multi-colored immunochromatography using nanobeads for rapid and sensitive typing of seasonal influenza viruses. *J. virol. methods* **209**, 62–68 (2014).
22. Fang, C.-C. et al. "Multiplexed detection of tumor markers with multicolor polymer dot-based immunochromatography test strip,". *Anal. Chem.* **90**, 2134–2140 (2018).

23. Cheng, X. et al. Rapid and quantitative detection of C-reactive protein using quantum dots and immunochromatographic test strips. *Int. J. Nanomed.* **2**, 5619–5626 (2014).
24. Choi, J. R. et al. "Lateral flow assay based on paper–hydrogel hybrid material for sensitive point-of-care detection of dengue virus,". *Adv. Healthc. Mater.* **6**, 1600920 (2017).
25. Rivas, L., Medina-Sánchez, M., De La Escosura-Muñiz, A. & Merkoçi, A. "Improving sensitivity of gold nanoparticle-based lateral flow assays by using wax-printed pillars as delay barriers of microfluidics,". *Lab. Chip.* **14**, 4406–4414 (2014).
26. Eriksson, E. et al. "Geometric flow control lateral flow immunoassay devices (GFC-LFIDs): a new dimension to enhance analytical performance,". *Research* https://doi.org/10.34133/2019/8079561 (2019).
27. Kainz, D. M., Früh, S. M., Hutzenlaub, T., Zengerle, R. & Paust, N. "Flow control for lateral flow strips with centrifugal microfluidics,". *Lab Chip* **19**, 2718–2727 (2019).
28. Hwang, H., Kim, S.-H., Kim, T.-H., Park, J.-K. & Cho, Y.-K. Paper on a disc: balancing the capillary-driven flow with a centrifugal force. *Lab Chip* **11**, 3404–3406 (2011).
29. Shen, M., Chen, Y., Zhu, Y., Zhao, M. & Xu, Y. Enhancing the sensitivity of lateral flow immunoassay by centrifugation-assisted flow control. *Anal. Chem.* **91**, 4814–4820 (2019).
30. Shen, M., Li, N., Lu, Y., Cheng, J. & Xu, Y. An enhanced centrifugation-assisted lateral flow immunoassay for the point-of-care detection of protein biomarkers. *Lab Chip* **20**, 2626–2634 (2020).
31. Khelifa, L., Hu, Y., Jiang, N. & Yetisen, A. K. Lateral flow assays for hormone detection. *Lab Chip* **22**, 2451–2475 (2022).
32. Ye, Y. et al. Development of a combined human transferrin-hemoglobin lateral immunochromatographic assay for accurate and rapid fecal occult blood test. *Clin. Lab.* **64**, 805–813 (2018).
33. Li, Z., Chen, H. & Wang, P. Lateral flow assay ruler for quantitative and rapid point-of-care testing. *Analyst* **144**, 3314–3322 (2019).
34. Hsieh, H. V., Dantzler, J. L. & Weigl, B. H. Analytical tools to improve optimization procedures for lateral flow assays. *Diagnostics* **7**, 29 (2017).
35. Parolo, C. et al. Tutorial: design and fabrication of nanoparticle-based lateral-flow immunoassays. *Nat. Protoc.* **15**, 3788–3816 (2020).
36. Wang, Z. & Ma, L. Gold nanoparticle probes. *Coord. Chem. Rev.* **253**, 1607–1618 (2009).
37. Lin, C.-C., Yang, Y.-M., Chen, Y.-F., Yang, T.-S. & Chang, H.-C. A new protein a assay based on Raman reporter labeled immunogold nanoparticles. *Biosens. Bioelectron.* **24**, 178–183 (2008).
38. Yuan, W. et al. A SERS nanocellulose-paper-based analytical device for ultrasensitive detection of Alzheimer's disease,. *Anal. Chim. Acta* **1301**, 342447 (2024).
39. Amendola, V. & Meneghetti, M. Size evaluation of gold nanoparticles by UV–vis spectroscopy. *J. Phys. Chem. C.* **113**, 4277–4285 (2009).
40. Haiss, W., Thanh, N. T., Aveyard, J. & Fernig, D. G. Determination of size and concentration of gold nanoparticles from UV– Vis spectra. *Anal. Chem.* **79**, 4215–4221 (2007).
41. Zhan, L. et al. The role of nanoparticle design in determining analytical performance of lateral flow immunoassays. *Nano Lett.* **17**, 7207–7212 (2017).
42. Zhou, G., Mao, X. & Juncker, D. Immunochromatographic assay on thread. *Anal. Chem.* **84**, 7736–7743 (2012).
43. Cho, S. Y., Park, T. S. & Lee, H. J. Interference of luteinizing hormone in the urinary point-of-care human chorionic gonadotropin test. *Clin. Chem. Lab. Med.* **51**, e149–e150 (2013).
44. Ren, W.-q. et al. "based analytical device for fast colorimetric detection of total hemoglobin and free hemoglobin from human blood sample,". *Microchem. J.* **187**, 108380 (2023).
45. Findlay, J. W. & Dillard, R. F. Appropriate calibration curve fitting in ligand binding assays. *AAPS J.* **9**, E260–E267 (2007).